Validation of 5G METIS map-based channel model at mmWave bands in indoor scenarios

Ines Carton[1], Wei Fan[1], Pekka Kyösti[2], Gert F. Pedersen[1]
[1]Department of Electronic Systems, Aalborg University, Aalborg, Denmark. Email: icl, wfa, gfp@es.aau.dk
[2]Anite Telecoms, Oulu, Finland. Email: pekka.kyosti@anite.com

***Abstract*—Valid channel models for the future generation of communications (5G) are paramount for system design and performance analysis. The METIS map-based model is based on 3D ray tracing principles with a simplified description of the environment and it is suitable for 5G communications. In this paper, the model is first described and then validated through comparison with indoor measurements performed at mmwave frequencies. Specifically, the dominant paths trajectory and power values are compared for three relevant scenarios: line of sight (LOS), non-line of sight (NLOS) and obstructed line of sight (O-LOS), where an object blocks the LOS path. Agreement between simulations and measurements is remarkable.**

***Index Terms*—METIS map-based model, ray tracing, millimeter wave, channel sounding, channel modeling and radio propagation.**

I. Introduction

The demand for ubiquitous, reliable and high-speed wireless connectivity has been steadily growing. It is anticipated that wireless data will grow around a tenfold by 2020 [1]. In 5G communication systems, it is expected an avalanche of traffic growth, an explosion of the number of connected devices and a large diversity of use cases and requirements. To face those challenges, a number of new features are targeted in the air interface design, e.g., small cellular cells, ultra-dense networks, movable base stations, device-to-device links, explorations of unused frequency spectrum above 6 GHz, and massive MIMO technologies [2].

Accurate channel characterization is important for system design and performance analysis. The following requirements were identified for 5G channel models in the METIS project [2], [3]:

- Exploration of unused frequency spectrum above 6 GHz.
- Utilization of ultra high bandwidth.
- Necessity of full 3D polarimetric channel models.
- Necessity of suitable models for massive MIMO, e.g., spherical wavefronts, spatial non-stationarity over large antenna arrays.
- Necessity of channel models for dynamic scenarios, e.g., device to device, machine to machine and vehicle to vehicle communications.
- Necessity of channel models compatible for various propagation scenarios.

Unfortunately, none of the existing channel models can address all 5G channel model requirements. A novel map-based channel model was proposed within the METIS project to address the requirements in 5G channel models [4]. The map-based model is based on ray tracing principle using a simplified 3D geometric modeling of the propagation environment. Propagation mechanisms, e.g. line-of-sight propagation, diffraction, specular reflection, diffuse scattering and blocking are implemented. Conventional ray tracing simulations often are subject to high complexity due to the use of a high-resolution database and high computation time associated with the ray trajectory identification. Moreover, ray tracing models are strictly site-specific, and hence results might not be applicable and sufficient for system level evaluations. To address these issues, random objects, which represent cars or humans for example, are introduced in the METIS map-based model. The complexity is also scalable, as number of rays and types of relevant propagation mechanisms can be predefined.

METIS map-based channel model is a promising candidate, since it fulfills the 5G channel modeling requirements [2]. However, validation of the implemented algorithms (i.e. path trajectory identification and propagation mechanism implementation) is missing. This paper targets to contribute in this aspect, by comparing METIS map-based channel models to channel sounding results in indoor scenarios. Note that the METIS map-based channel model does not intend to work as a deterministic ray tracing tool, and hence the comparison in this work only attempts to verify whether the above-mentioned algorithms in the METIS map-based model are implemented as expected. To do so, measurements in an static indoor scenario at mmwave frequencies are compared with the results extracted from the METIS map-based model.

The paper is organized as follow. Section II briefly introduces the METIS map-based channel model. In section III, the measurement setup and measurement scenarios are described. Comparison results between the METIS map-based channel model and the measurement results are shown in Section IV. Finally, section V concludes the paper.

II. METIS Map-Based Model

The METIS map-based model is based on 3D ray tracing principle. The model targets both spatial and frequency consistency by using a simplified geometric description of the environment and well-established frequency dependent formulas to describe the propagation effects [4]. Seven representative scenarios expected in future cellular communication systems are defined, e.g., urban micro cell, urban macro cell, indoor

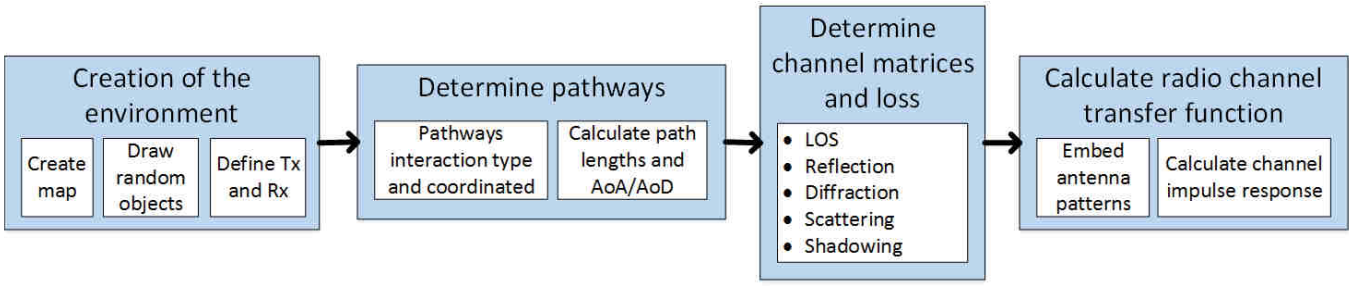

Fig. 1. Block diagram of METIS map-based model. [4].

office, indoor shopping mall, highway, open air festival and stadium.

A block diagram of the METIS map-based model is illustrated in Fig. 1. Step-by-step instructions of how the METIS map-based model works are detailed in [4] and only outlined here. The first step of the model is to create the propagation environment. Buildings are composed by walls which are represented as rectangular surfaces with certain electromagnetic properties. These surfaces are then divided into tiles, where the tile center corresponds to a potential diffuse scattering source. The model allows to define objects, which could correspond to, for example, people, vehicles, trees, etc. The height and width of the objects can be defined and they are distributed around the environment either following a regular pattern, e.g., in the stadium scenario, or randomly according to a certain density. These objects have a twofold role in the propagation; they may block a path producing shadowing or act as a scatterer node. Once the random objects are distributed across the environment, the model is purely deterministic.

The next step is to find the possible path ways from each Tx to each Rx location. Possible interactions with the environment are: line of sight (LOS), reflections, corner diffractions, over the roof top propagation, shadowing by objects, scattering by objects, penetration through building walls, and diffuse scattering. Once the possible path ways are determined, each path length, and angles of departure and arrival are calculated.

After the pathways are identified, the next step is to determine the propagation channel matrices for the path segments, i.e., calculate the losses due to the different interactions and polarization matrices. Contrary to other existing channel models, path loss and shadowing are not explicitly modelled by empirical distributions in the METIS map-based model. Alternatively, these effects are determined by the contribution of the different propagation paths. Below, there is a brief description of each of these propagation mechanisms:

- **Direct LOS:** For direct LOS, the path loss is modeled by Friis equation.
- **Specular reflection:** Only a fraction of the incident power is reflected. This is defined by the parameter β, which is the ratio between the reflected and the scattered power. The β parameter can be either predefined or alternatively calculated based on the surface roughness effect [5]. The channel matrix for reflections is calculated according to the Fresnel reflection coefficients for electric fields [6].
- **Diffraction:** Two models are used to model diffraction around edges: uniform theory of diffraction (UTD) [7], and Berg's model [8]. Note that Berg's model is applied for estimating path loss in urban microcell environments, and hence not considered in our indoor investigation.
- **Shadowing due to object blocking:** To model shadowing, the objects are modeled as rectangular screens with a predefined height and width. Two cases are considered to model shadowing by objects: low and high object density. In the former, shadowing is calculated as the knife-edge diffraction around the four edges of the screen [4]. For the latter, shadowing is modelled using the Walfisch-Bertoni model [9].
- **Scattering from objects:** In this case, objects do not act as rectangular screens anymore. Instead, the scattering loss produced by an object is modelled based on the scattering cross section for a perfect conducting sphere [4].
- **Diffuse scattering:** The density of the source distributions for diffuse scattering is configurable through the tile size. Just like for specular reflections, the scattered power is defined either by the parameter β or the surface roughness effect. The walls from the room where the measurements were performed and relatively smooth. Diffuse scattering barely appears in the measurement results and, hence, is not discussed in this paper.
- **Penetration loss:** Penetration is not considered in this paper. Penetration losses at mmwave bands are very high, and hence paths that penetrate the walls would not be present in our measurements.
- **Over the rooftop propagation:** Since our measurements are performed in an indoor environment, over the roof top propagation is not relevant to the paper.

Finally, antenna patterns are embedded into the result and the final channel impulse responses are calculated. Note that the number of path ways are scalable to limit the computational complexity. Pathway identification is detailed in [4].

The purpose of this paper is to validate the pathway identification algorithm and the implementation of the propagation loss calculation in the METIS map based model. Note that only some propagation mechanisms can be validated with our indoor measurements, as explained above.

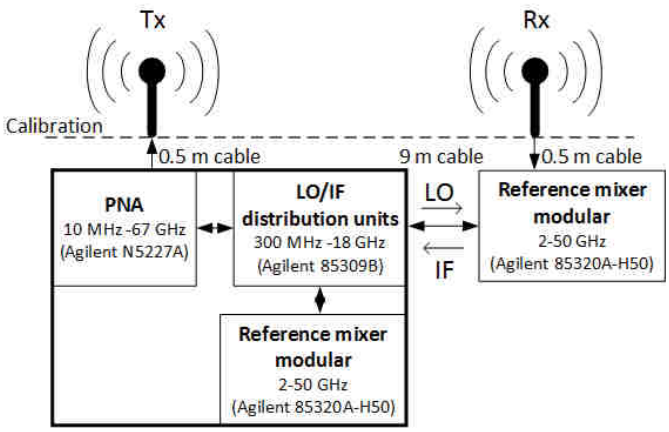

Fig. 2. Block diagram of the measurement setup. The reference mixer modular is used to down-convert the signal from the Rx to reduce cables losses. Calibration was performed to de-embed the Tx and Rx chain from the measurements.

TABLE I
TX AND RX ANTENNAS SPECIFICATION

Antenna	Freq. range	Gain	Pattern
Biconical	2-30 GHz	6 dB	Omnidirectional
Horn	26.4-40.1 GHz	19 dB	HPBW = 20 deg

III. MEASUREMENTS DESCRIPTION

A. Measurement Setup

Fig. 2 shows a block diagram of the measurement system. A biconical antenna was used at the transmitter (Tx) side, whereas a horn antenna was used at the receiver (Rx) side. Both Tx and Rx antenna are placed at the same height and are vertically polarized. The main characteristics of the antennas are summarized in Table I. The Rx is placed on the center of a turntable. A full sweep over 360 degrees with steps of 10 degrees for scenario 1 and 2 and 0.5 degrees for scenario 3 is performed. Applying the inverse Fourier transform to each frequency sweep, the power angular delay spectrum can be calculated. The central frequency used for the measurements is 29 GHz with a bandwidth of 2 GHz. For this bandwidth, the delay resolution is 0.5 ns. Moreover, 750 frequency points were recorded for the frequency range 28-30 GHz, resulting into a delay range of 350 ns.

B. Measurement Scenarios

To allow a clear comparison, measurements were performed in a static indoor environment where no furniture was present. Although all measurements were performed in the same room, three different scenarios were used as pictured in Fig. 4, 6 and 8, namely line-of-sight (LOS), non-LOS (NLOS), and obstructed LOS (O-LOS). These three scenarios were selected in order to investigate different propagation mechanisms, e.g., LOS, reflection, diffraction, or scattering. The walls of the room are made of concrete and the blackboard used in the O-LOS scenario to obstruct the LOS has one side covered by aluminum. The dimensions of the blackboard are 1.19 m $\times$ 1.19 m. Fig. 3 shows a picture of the scenarios for the O-LOS (left) and NLOS (right) cases. Note that in the O-LOS case, a wooden board was present in the room. For the LOS and NLOS scenarios, the height of the antennas was 0.84 m, whereas for the O-LOS scenario the antennas' height was 1.1 m.

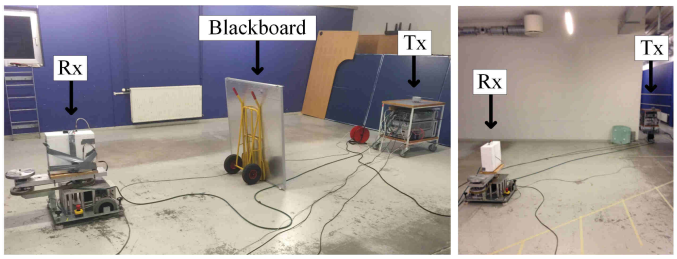

Fig. 3. Picture of the room where the measurements were taken. O-LOS scenario is shown on the left where the right wall of the room can be seen as well as the wooden board placed at the bottom. The picture on the right show the NLOS case without the wooden board.

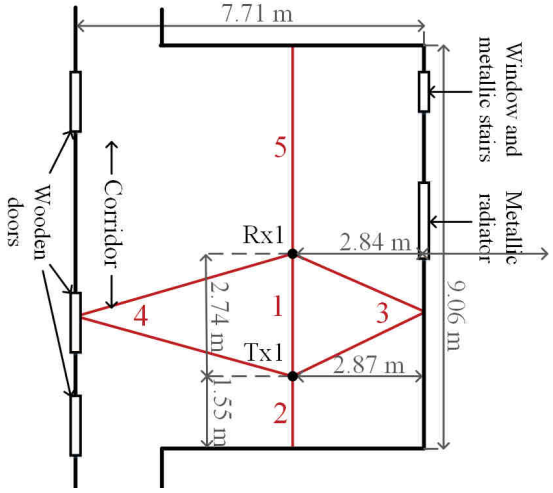

Fig. 4. Scenario 1: LOS. Room geometry and main paths are shown.

IV. RESULTS COMPARISON

In order to compare the measurement with the METIS map-based model results, the scenarios depicted in Fig. 4, 6 and 8 where modelled with the METIS implementation. The most relevant paths identified with the METIS model are shown in the referred figures. The comparison is done in terms of power per identified path.

A. LOS scenario

The power-angular-delay spectrum for the LOS case, is shown in Fig 5. It can be seen that only a few dominant components can be identified. The LOS component is dominant, as expected. Path trajectories can be identified, by matching the delay and angle of arrival of each component to the room geometry shown in Fig. 4. The trajectories of the main paths

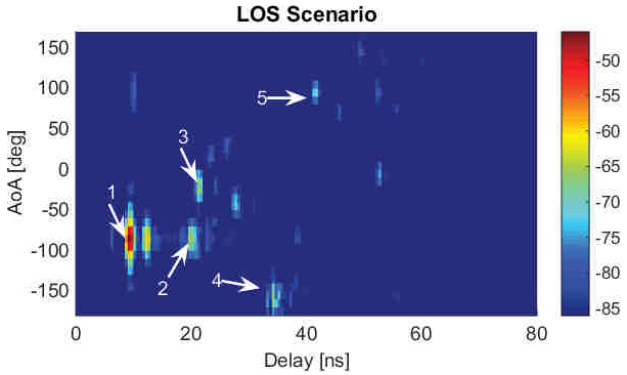

Fig. 5. Power angular delay spectrum for scenario 1, LOS.

TABLE II
PATH POWER IN THE LOS SCENARIO.

LOS	#1	#2	#3	#4	#5
Meas [dB]	-46.03	-65.82	-66.12	-67.28	-70.44
METIS [dB]	-46.55	-65.03	-66.66	-70.10	-71.48
Diff [dB]	0.52	-0.79	0.54	2.82	1.04
Path	LOS	Ref	Ref	Ref	Ref

TABLE III
PATH POWER IN THE NLOS SCENARIO.

NLOS	#1	#2	#3
Meas [dB]	-75.88	-71.80	-73.06
METIS [dB]	-78.235	-73.05	-74.21
Diff [dB]	2.35	1.25	1.15
Path	Dif	Ref	Ref

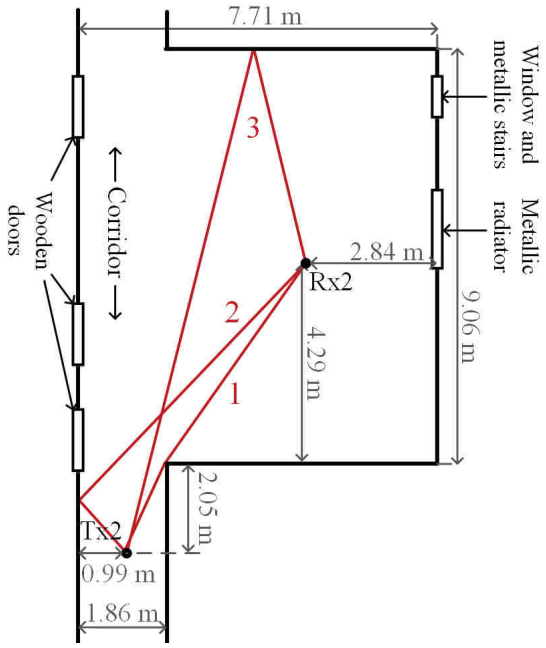

Fig. 6. Scenario 2: NLOS. Room geometry and main paths are shown.

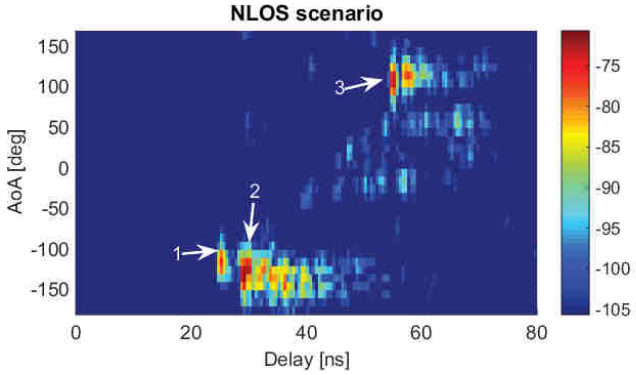

Fig. 7. Power angular delay spectrum for scenario 2, NLOS.

the path trajectories identified by the METIS map based model are shown in Fig. 4, which agree with the paths identified in the measurement results.

The first two paths imping the Rx at -90 degrees (#1 and #2) are identified to be the LOS component, and a reflection from the bottom wall behind the Tx. The paths numbered as 3, 4, and 5 are reflections on the left wall, on the right wall, and on the upper wall, respectively. Table II shows the power of these components extracted from the measurements and from METIS map-based model, as well as the deviations between them. Note that the maximum gain from the antennas has been considered in the results from the METIS model to have a fair comparison. A reasonable agreement is achieved between the measurement and the METIS simulation, with a maximum deviation up to 2.8 dB.

B. NLOS scenario

Fig. 7 shows the power-angular spectrum for the NLOS scenario. In this case, the transmitter is placed behind a corner and the direct LOS component is blocked as shown in Fig. 6. It can be seen in Fig. 6 that there are long tails in delay following the main paths, which are most likely paths due to multiple reflections on the walls and diffuse components. With the METIS map-based model, only three main paths are identified: the corner diffraction (#1), reflection with the left wall (#2), and reflection with the upper wall (#3). This is due to the fact that only single reflections are defined in the model. The power values of the three paths are shown in Table III. The power values agreement is good between measurements and simulation, with a deviation up to 2.4 dB.

C. O-LOS Scenario

O-LOS was selected to evaluate the scattering produced by random objects in the METIS map based model. An object is deliberately placed at the same position to evaluate the losses produced by scattering. Fig. 9 shows the measured power-angular-delay spectrum. Three main paths are identified with

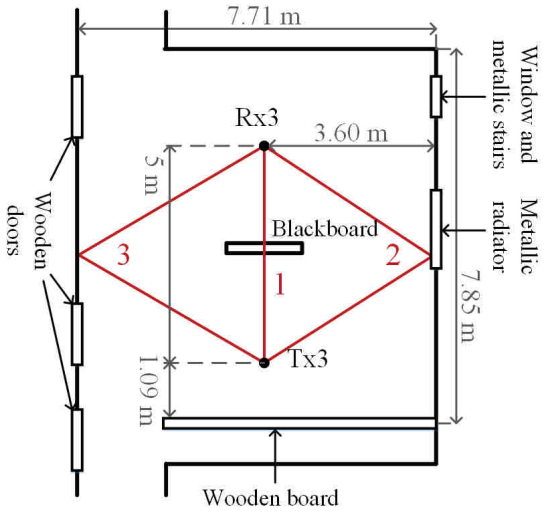

Fig. 8. Scenario 3: O-LOS. Room geometry and main paths are shown.

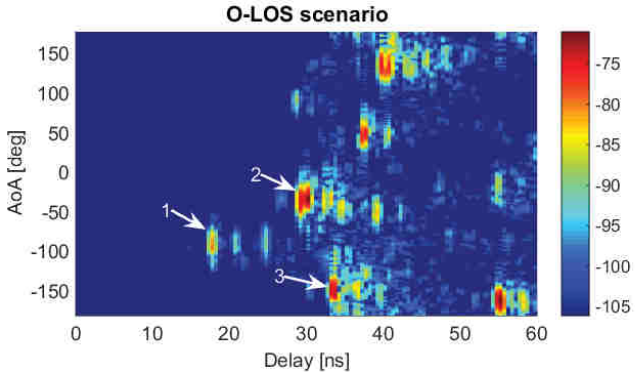

Fig. 9. Power angular delay spectrum for scenario 3, O-LOS.

TABLE IV
PATH POWER IN THE O-LOS SCENARIO.

O – LOS	#1	#2	#3
Meas [dB]	-79.96	-71.08	-73.43
METIS [dB]	-80.87	-70.61	-70.95
Diff [dB]	0.91	-0.47	-2.48
Path	Scat	Ref	Ref

the METIS map based model as shown in Fig. 8. It can be seen that there are a few dominant paths (at around 40 ns delay and 55 ns delay) present in the measurements, which are not identified with the METIS simulation. This is due to the fact that second-order reflections, which are dominant in this O-LOS scenario, are not evaluated. It can be seen that the path incoming from where the blackboard is placed are significantly attenuated, i.e., #1. The paths numbered as #2 and #3 correspond to first order reflections on the right and left walls respectively. Table IV shows the power values for each of these paths.

V. CONCLUSIONS

The METIS map-based model, which utilizes ray-tracing principles to model the environment, has been described in this paper. To validate the implementation of the model, simulation results have been compared with measurements in indoor scenarios. Three scenarios within the same room where selected for the validation, i.e., LOS, NLOS, and O-LOS. These where selected to validate the implementation of different propagation mechanisms, namely, LOS paths, specular reflections, diffractions and object scattering.

The main paths distinguished in the measurement results are successfully identified by the model for the LOS and NLOS scenarios. Double reflections become important for the O-LOS scenario, where the LOS component is obstructed. Furthermore, the power values from these main paths were also compared reaching acceptable agreement between simualtions and measurements, i.e., deviations up to 2.8 dB.

One possible extension of the work would be to perform further measurements to validate other propagation mechanisms, such as blocking by objects or penetration through walls. However, since the model is meant to be used with simplified and generic propagation environments, it would be of greater interest to compare other channel statistics or validate that the model is consistent through frequency.

ACKNOWLEDGMENT

This work has been supported by the Danish High Technology Foundation via the VIRTUOSO project. The authors would like to thank Kristian Bank, Yi Tan, Kim Olesen, and Anders Karstensen for their assistance with the measurements.

REFERENCES

[1] Ericsson, "Ericsson mobility report," June 2015. [Online]. Available: http://www.ericsson.com/mobility-report

[2] "Scenarios, requirements and KPIs for 5G mobile and wireless system," Mobile and wireless communications Enablers for the Twenty-twenty Information Society (METIS), Deliverable D1.4 ICT-317669-METIS/D1.1, Apr. 2013.

[3] J. Medbo, K. Borner, K. Haneda, V. Hovinen, T. Imai, J. Jarvelainen, T. Jamsa, A. Karttunen, K. Kusume, J. Kyrolainen, P. Kyosti, J. Meinila, V. Nurmela, L. Raschkowski, A. Roivainen, and J. Ylitalo, "Channel modelling for the fifth generation mobile communications," in *Antennas and Propagation (EuCAP), 2014 8th European Conference on*, April 2014, pp. 219–223.

[4] "METIS Channel Models," Mobile and wireless communications Enablers for the Twenty-twenty Information Society (METIS), Deliverable D1.4 ICT-317669-METIS/D1.4, Feb. 2015.

[5] O. Landron, M. J. Feuerstein, and T. S. Rappaport, "A comparison of theoretical and empirical coefficients for typical exterior wall surfaces in a mobile radio environment," *IEEE Transactions on Antennas and Propagation*, vol. 44, pp. 341 – 351, Mar. 1996.

[6] R. G. Vaughan and J. B. Andersen, *Channels, Propagation and Antennas for Mobile Communications*. IET, 2003.

[7] D. A. McNamara, C. W. I. Pistorius, and J. A. G. Malherbe, *Introduction to The Uniform Theory of Diffraction*. Norwood, MA: Artech House, 1990.

[8] J. E. Berg, "A recursive method for street microcell path loss calculations," in *Sixth IEEE International Symposium on Personal, Indoor and Mobile Radio Communications, 1995. PIMRC'95. Wireless: Merging onto the Information Superhighway*, Sept 1995, pp. 140–143.

[9] J. Walfisch and H. L. Bertoni, "A theoretical model of uhf propagation in urban environments," *IEEE Transactions on Antennas and Propagation*, vol. 36, pp. 1788–1796, Dec. 1988.